2014-07-10

Combustion Characterization and Ignition Delay Modeling of Low- and High-Cetane Alternative Diesel Fuels in a Marine Diesel Engine

Petersen, John

American Chemical Society

energy&fuels

Article

pubs.acs.org/EF

Combustion Characterization and Ignition Delay Modeling of Low- and High-Cetane Alternative Diesel Fuels in a Marine Diesel Engine

John Petersen, Doug Seivwright, Patrick Caton,*,† and Knox Millsaps

Mechanical and Aerospace Engineering Department, U.S. Naval Postgraduate School, Watkins Hall 700 Dyer Road Monterey, California 93943-5100, United States

ABSTRACT: In support of an ongoing U.S. Navy alternative fuel evaluation program, the combustion characteristics of two very different alternative diesel fuels were evaluated in a direct-injection marine diesel engine across a variety of speeds and loads. The fuels were an algal-based hydrotreated renewable diesel fuel (HRD) with cetane number of ∼75 and a synthetic paraffinic kerosene (SPK) with cetane number of ∼25. These fuels were experimentally tested as blends with conventional petroleum-based military diesel fuel (designated F-76) with cetane ≈ 46, giving a cetane number range from 25 to 75. Start of injection (SOI) was characterized using a strain gauge to determine actuation of the mechanical unit injector; SOI remained essentially unchanged for changes in fuel type. As expected based on cetane number, ignition delay (IGD) increased with greater amounts of SPK fuel and decreased for greater amounts of HRD fuel in the test blend. Energy release analysis showed that longer IGD led consistently to slightly advanced combustion phasing, as indicated by the location of 50% mass fraction burned, decreased overall combustion duration, and greater maximum rate of pressure rise due to greater fuel-air premixing. Fuel consumption was 0−5% higher for these alternative fuels. Ignition delay was modeled using a detailed primary reference fuel mechanism tuned to match the measured cetane number of each neat and blended fuel. The modeled chemistry was able to capture relative changes in the experimentally observed IGD, suggesting that the measured differences in physical properties, which will affect spray development, do not contribute as significantly to differences in IGD. The results suggest that typical higher cetane alternative fuels, such as HRD, have no deleterious effects from the perspective of combustion characteristics. Processes that yield lower cetane alternative fuels, such as SPK, while still achieving satisfactory performance, begin to show signs of problems through delayed combustion, increased rates of pressure rise, and higher peak pressures, which induce higher mechanical stress and combustion noise.

INTRODUCTION

Developing viable future alternatives to petroleum-based fuels is of continued high importance for civilian and military prime movers. From a military perspective, the Department of Defense is the single largest consumer of energy in the U.S., using approximately two percent of the U.S. petroleum demand.[1] In 2009, the U.S. Navy outlined the several important energy goals, including an alternative-fueled carrier strike group (2016) and a 50% alternative-fuel energy portfolio by 2020.[2]

Given the prevalence and longevity of diesel engines in service, widespread redesign or replacement to accommodate possible future variations in fuels is unlikely. Future fuels will therefore need to be compatible with present technology. Understanding how future fuels will perform in current and legacy technology diesel engines is important for qualification and acceptance of candidate fuels. However, there is currently little consensus as to the exact nature of what future alternative diesel fuels will be.

There are, however, some generalizations that can be made about likely future fuels. The first generation of alternative diesel biofuel, known as biodiesel, is produced by the transesterification of triglycerides (often from vegetable oils or animal fats) into fatty acid methyl esters (FAMES) or fatty acid ethyl esters. Biodiesel has entered the commercial marketplace and is currently a common additive to civilian diesel fuel. However, biodiesel blends are not used in U.S. Navy engines due to many issues, including microbial contamination and the formation of fuel-water emulsions from seawater-ballasted storage tanks.[3]

Beyond biodiesel, next-generation diesel alternative fuels are typically produced via catalytic processes and result in highly paraffinic (saturated) hydrocarbons with variable degrees of branching. Fischer−Tropsch process fuels (FT) or hydrotreated fuels (hydrotreated renewable diesel, HRD) often exhibit higher cetane numbers than conventional petroleum diesel fuel.[4,5] Experimental work with these fuels in diesel engines has shown largely satisfactory performance.

Sugiyama et al. tested HRD in a direct injection turbocharged automotive diesel and observed decreased hydrocarbon emissions with reduced fuel consumption of up to 5% compared to conventional diesel.[6] Kuronen et al. compared HRD to conventional (sulfur-free) diesel in heavy-duty diesel engines and noted lower emissions and a 1−2% decrease in fuel consumption.[7] Aatola et al. found similar results and concluded that better improvements could be achieved with engine optimization for fuel.[8] Caton et al. tested HRD in a military indirect injection engine used in the high mobility multipurpose wheeled vehicle (HMMWV) and noted shorter ignition delay (IGD) and longer combustion duration.[9]

Received: March 20, 2014
Revised: July 8, 2014
Published: July 10, 2014

   dx.doi.org/10.1021/ef500565t | *Energy Fuels* 2014, 28, 5463−5471

These studies demonstrate the viability and potential effects of one particular potential alternative diesel fuel, but more work needs to be done to anticipate how a range of possible future fuels might perform in existing technology. In one study, Cowart et al. investigated a series of alternative fuels and pure component fuels spanning a cetane number range from 44 (military F-76 petroleum diesel) to 100 (*n*-hexadecane), noting in particular the effects of fuel reactivity and density on IGD and other performance metrics, but finding overall satisfactory performance. However, this study was done using an indirect injection diesel engine that may be uncharacteristic for typical diesel engines, which utilize direct injection.[10] Olree and Lenane tested fuels with cetane numbers ranging from 35 to 55, and observed that shorter IGD led to less fuel-air premixing and lower rates of maximum pressure rise.[11] Another study compared the IGDs of 20 pure component fuels with a very wide range of cetane numbers (from negative values to 100), but again using a single-cylinder indirect injection research diesel engine, which may not be representative of most production diesel engines.[12]

Given the limited experimental data representative of possible future diesel fuels in typical direct-injection diesel engines, the objective of this study is to test synthetic diesel fuels over a wider range of cetane numbers using a direct-injection diesel engine. The present work utilizes two candidate highly paraffinic fuels with very different cetane numbers. Algal-based HRD fuel with a cetane number of approximately 75 and a synthetic paraffinic kerosene fuel (SPK) with a cetane number of approximately 25 are tested in blends with petroleum-based U.S. Navy diesel fuel designated F-76. The resulting cetane number range of 25−75 is likely characteristic of many possible future fuels. Furthermore, these alternative fuels are not pure components but realistic candidate fuels with a variety of components, albeit far fewer than conventional petroleum-based fuels. This study utilizes a direct-injected marine diesel engine, characteristic of many of the legacy diesel engines that will be in service for many years to come.

This study also seeks to utilize an available primary reference fuel chemistry model to determine the degree to which it could be used to predict future fuel performance with only basic compositional information about the fuel. A precise chemistry model for future fuels could not be constructed without knowledge of fuel composition. However, diesel fuels can often be represented by a mixture of reference fuels, such as binary blends of heptamethylnonane (*i*-$C_{16}H_{34}$, highly branched, saturated C16) and normal hexadecane (*n*-$C_{16}H_{34}$, straight-chain, saturated C16). Since future fuels from catalytic processes will also likely be highly paraffinic in character with variable degrees of branching, the primary reference fuel approach may also be a good way to model the behavior of these alternative fuels. Cowart et al. take this approach in an attempt to model HRD performance and conclude that a 65:35 blend of *n*-$C_{16}H_{34}$/*i*-$C_{16}H_{34}$ is a good surrogate for the HRD ignition behavior.[13] An additional objective of the present study is to determine the extent to which an existing chemistry model could predict important parameters such as IGD of the wide range of fuel cetane number tested in this study.

EXPERIMENTAL SECTION

Engine testing was conducted in a Detroit Diesel 3−53 engine connected to a Superflow SF-901 water-brake dynamometer system. The engine is a three cylinder in-line, two-stroke engine often used for marine propulsion applications. Characteristics of the engine are given in Table 1. Direct injection is accomplished by mechanical unit injectors actuated by an injection timing camshaft lobe. A supercharger provides modest boost (3−22 kPa abs). Air was metered using a turbine flow meter in the inlet air stream. Intake airbox pressure, after the supercharger, was measured using a static pressure sensor. In-cylinder pressure was measured using a Kistler type 6125A piezocapacitive transducer with a Kistler dual mode 5010 charge amplifier. Crank angle position measurement was accomplished using a BEI optical encoder model DHM5 with 0.5° resolution mounted directly to the engine crankshaft. Fuel flow rate was measured using a fuel weight measurement system and an ETAS LA4 wide-band oxygen sensor mounted in the exhaust flow. The experimental setup is shown in Figure 1.

Table 1. Engine Characteristics and Experimental Conditions

type	direct-injection diesel, three cylinder in-line, two-stroke, supercharged
bore × stroke	98.4 × 114 mm (3.875 × 4.50 in)
piston-bore clearance	0.51 mm (0.020 in)
speed	550, 1100, 1650, 2200 rpm
R_v	21
boost	3−22 kPa (0.4−3.2 psi)
peak power	75.3 kW (101 hp) at 2800 rpm
peak torque	278 N·m (205 ft·lbf) at 1560 rpm
intake air	lab ambient, 22 °C
fuel	U.S. Navy F-76 petroleum-based diesel
	synthetic paraffinic kerosene (SPK)
	algal-based hydrotreated renewable diesel (HRD)
	blends of F-76 with each alternative fuel

To confirm potential changes in the start of injection timing with load, speed, and fuel changes, a strain gauge was mounted to the fuel injector rocker arm on one of the cylinders. A Micro-Measurements model WK-06−062TT-350 tee rosette strain gauge was mounted in a half-bridge configuration on the rocker arm to provide strain data

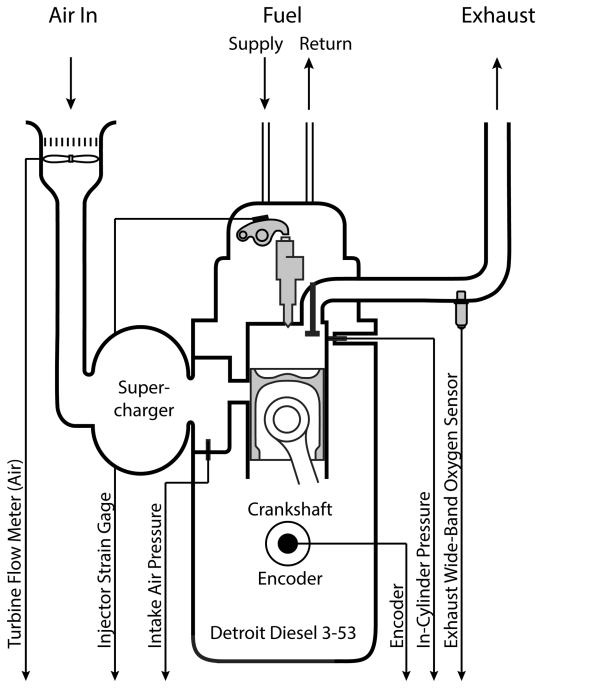

Figure 1. Experimental setup of Detroit Diesel 3−53 engine showing air, fuel, and exhaust flows along with the main sensors used in this study.

dx.doi.org/10.1021/ef500565t | *Energy Fuels* 2014, 28, 5463−5471

independent of temperature changes. A stand-alone computer running LabVIEW 2010 software and two NI DAQ boards, namely, NI PCI-6281 and NI PCI-6602 (counter-timer specific board), were used to acquire data signals from the engine setup.

The engine was operated at 10 different operating conditions throughout its speed-load operating range; these operating points are indicated and numbered in Table 2. Most of the experimental analysis

Table 2. Speed and Torque Operating Points Numbered 1−10 of the Test Engine

	speed, RPM			
torque N·m (ft·lbf)	550	1100	1650	2200
68 (50)	1	2	5	
136 (100)		3	6	9
203 (150)		4	7	10
258 (190)			8	

in this study was subsequently done using operating points 3, 8, and 10, which nominally represent a midload "cruise" condition, a high-torque condition, and a high-power condition, respectively.

Table 3 gives measured properties of the three fuels utilized in this study. F-76 is the U.S. Navy designation for petroleum-based diesel

Table 3. Properties of F-76, HRD, and SPK Fuels

	F-76	HRD	SPK
ρ (kg/m^3)[a]	844	778	760
σ (mN/m)[b]	25.8	24.9	26.8
μ (cSt)[c]	3.0	2.748	1.088
LHV[d] (MJ/kg)	42.7	44.0	44.0
cetane	46[e]	∼75	24.7
composition			
wt % C	86.8[e]	85.1[e]	84.8
wt % H	13.1[e]	14.9[e]	15.2
wt % O	0	0	0
wt % S	0.1[e]	0[e]	0
% paraffin	70.7	98.5	94.3
% olefin	2.3	0.9	4.7
% aromatic	27	0.6	1.0

[a]Properties measured at 15 °C. [b]Properties measured at 24 °C. [c]Properties measured at 40 °C. [d]LHV = lower heating value. [e]Properties measured by Southwest Research Institute, Oct 2012 and Feb 2013, or by Naval Air Systems Command, Fuels Division, Patuxent River, MD.

fuel. HRD indicates a hydrotreated renewable diesel fuel derived from algae and currently under testing by the U.S. Navy. The SPK fuel is a synthetic paraffinic kerosene fuel and was obtained from the Wright Patterson Air Force Research Laboratories. The HRD was obtained from the Naval Air Systems Command, Fuels Division, Patuxent River, MD.

The ignition behavior of the fuels was modeled using a primary reference fuel chemistry model for diesel fuel. The model includes detailed chemistry for normal hexadecane (n-$C_{16}H_{34}$) and heptamethylnonane (i-$C_{16}H_{34}$), in particular, and includes chemistry of normal hydrocarbons up to C20. The model contains 4204 species and 20 235 reactions and was based on a diesel primary reference fuel (PRF) mechanism. This mechanism was built on the framework of a gasoline PRF mechanism by adding the chemistry associated with breaking down the diesel PRFs (heptamethylnonane and n-hexadecane) into species present in the gasoline PRF pathways. Validation was conducted using experimental studies of ignition in shock tubes and using jet-stirred reactors.[14] This base mechanism was then merged with an iso-alkane mechanism and extended for normal paraffins from C17−C20.[15−17] Ignition delay was modeled by considering a fuel-air parcel with constant enthalpy-pressure constraints at specified T, P, and composition (fuel composition and overall fuel-air equivalence ratio), which are described in the Results section. The chemistry rate equations were implemented in Matlab with Cantera, an open-source suite of functions that operates within the Matlab environment and facilitates thermodynamic and kinetic calculations.[18]

RESULTS

Figure 2 shows a typical pressure trace (top) and cumulative energy release (bottom) for operation of the test engine with

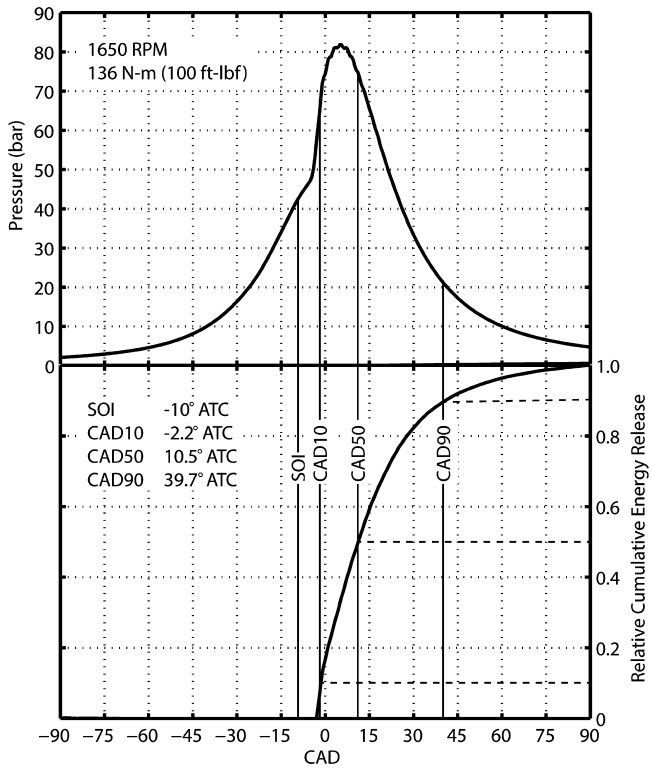

Figure 2. Pressure trace and relative cumulative energy release for operating point at 1650 rpm and 136 N·m (100 ft·lbf) indicating the measured values for SOI, CAD10, CAD50, and CAD90.

conventional petroleum-based F-76 fuel at operating condition 6 (1650 rpm, 136 N·m/100 ft·lbf of torque). This figure illustrates some of the typical properties used to compare operation of the fuels in this study and gives the typical performance of the test engine. Several important features are shown in the figure: the start of injection (SOI) is nominally 10° before top-center (BTC) or −10° after top-center (ATC), as indicated in the Figure. After a short IGD period, the pressure trace shows deviation from the approximately isentropic compression curve, and the cumulative energy release, shown in the bottom panel, indicates fuel is reacting and releasing chemical energy. The locations for 10%, 50%, and 90% mass fraction burned are shown in the Figure, abbreviated CAD10, CAD50, and CAD90, respectively, and are located at −2.2°, 10.5°, and 39.7° ATC.

Energy release is calculated from the experimentally measured pressure and volume using a first-law energy balance:

$$\frac{\delta E_{ch}}{dt} = \frac{\delta Q}{dt} + P\frac{dV}{dt} + mc_v\frac{dT}{dt}$$

Here, the δE_{ch} term is the chemical energy release. The δQ term is the heat transfer out of the combustion chamber as

dx.doi.org/10.1021/ef500565t | Energy Fuels 2014, 28, 5463−5471

estimated by the Woschni correlation.[19] The PdV term represents work from the engine, and the $mc_v dT$ term is the change in sensible energy inside the chamber as estimated by the change in temperature. The temperature is calculated from an ideal gas equation of state based on the measured temperature and pressure. The specific heat at constant volume, c_v, is calculated with temperature dependence assuming a constant composition of nitrogen using polynomial fits in Cantera.[18,20] This approach follows that of Gatowski et al. and Chun and Heywood, although the present approach includes temperature dependence of c_v and neglects any inflow or outflow terms, such as crevice flow.[21,22]

While Figure 2 gives explicit operating data for the test engine at a specific operating point, the majority of subsequent comparisons made in this study are done on a relative basis; for example, a test fuel blend is compared to operation with conventional F-76 at a particular operating condition. This relative basis directly addresses the present goal, which is to determine how these different yet viable alternative fuels will affect unmodified legacy diesel engines, originally designed for operation only with conventional diesel fuel. One critical quantity in this study is the IGD, defined here as the time delay between start of injection (SOI) and the start of combustion (SOC):

$$\mathrm{IGD} = \mathrm{SOC} - \mathrm{SOI}$$

For operation with two different test fuels at the same operating condition (referred to as *a* and *b* below for convenience), the relative change in IGD is

$$\Delta\mathrm{IGD} = \mathrm{IGD}_a - \mathrm{IGD}_b$$
$$= (\mathrm{SOC} - \mathrm{SOI})_a - (\mathrm{SOC} - \mathrm{SOI})_b$$

$$\Delta\mathrm{IGD} = (\mathrm{SOC}_a - \mathrm{SOC}_b) - (\mathrm{SOI}_a - \mathrm{SOI}_b)$$

Small changes in SOI, which may occur with operating conditions despite the fixed hardware that drives the fuel injector in the engine, can be detected with an instrumented fuel injector. In this study, a strain gauge was mounted to the rocker arm, which drives the fuel injector. The slope of the recorded strain gauge signal can be used to deduce changes in SOI timing.

Figure 3 shows the strain gauge signal for operation at operating point 6 (1650 rpm, 136 N·m/100 ft·lbf of torque) for operation with F-76, neat HRD, and neat SPK fuels. The nominal SOI of the engine is shown (−10° ATC) on the figure and occurs consistently just after the strain signal changes slope, indicating that fuel is being compressed in the injector. Note that all three fuels show essentially identical strain with crank position. Because SOI is insensitive to fuel type, the ($\mathrm{SOI}_a - \mathrm{SOI}_b$) term in the equation above can be neglected when comparing IGD between different test fuels at the same operating point.

Figure 4 shows the relative IGD ($\mathrm{IGD} - \mathrm{IGD}_{F76}$) at operating points 2−10. No attempt was made to delineate the trendlines on the on the Figure. The intent of the Figure is to show the general trend as fuel is changed. F-76−SPK blends are shown on the left side of the horizontal axis, with neat SPK operation on the left-most side of the axis. F-76−HRD blends are shown on the right side of the axis, with neat HRD operation on the right-most side. Operation with F-76 is indicated by "0%" in the middle of the horizontal axis. The data are presented in this way to allow a monotonically increasing

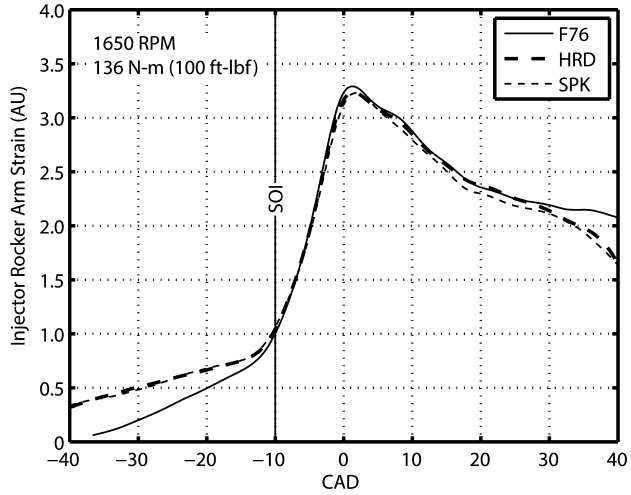

Figure 3. Strain gauge signal for characteristic operating point at 1650 rpm and 136 N·m (100 ft·lbf) for neat F-76, HRD, and SPK fuels showing similar strain increase profiles and therefore uniform SOI across fuel types at the same operating point.

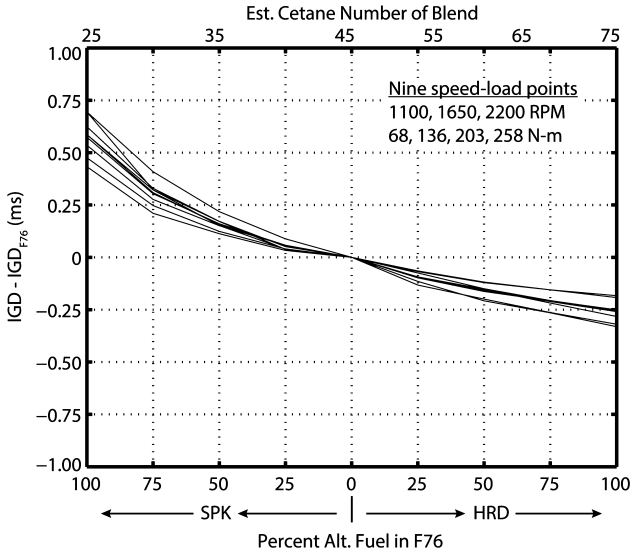

Figure 4. Changes in IGD relative to F-76 for various blending ratios of SPK and HRD with F-76 across nine operating points (speeds of 1100, 1650, 2200 rpm and loads of 68, 136, 203, 258 N·m). Estimated cetane number is shown on the upper horizontal axis.

cetane number from left to right on the horizontal axis. The estimated cetane number is shown on the upper horizontal axis, calculated by averaging the measured cetane number of the components of the fuel blend.

The data in Figure 4 show that IGD is highest for neat SPK operation and is 0.50 to 0.75 ms longer than operation with F-76. Ignition delay decreases monotonically as more F-76 is used in place of SPK and then as HRD replaces F-76. Neat HRD has the shortest IGD, approximately 0.25 ms faster than F-76 operation. These trends are consistent with increasing cetane number; the fuel blends are more reactive and begin to ignite sooner after injection into the combustion chamber.

Decreasing IGD means there is less time for the injected fuel to mix with air in the combustion chamber prior to the onset of ignition. After ignition, the quantity of fuel and air that have already mixed will burn very quickly, and can be called the *premixed fraction*.[23] Therefore, shorter IGD will often lead to

dx.doi.org/10.1021/ef500565t | *Energy Fuels* 2014, 28, 5463−5471

less premixed fraction and consequently to a longer overall combustion duration. Figure 5 shows combustion duration in

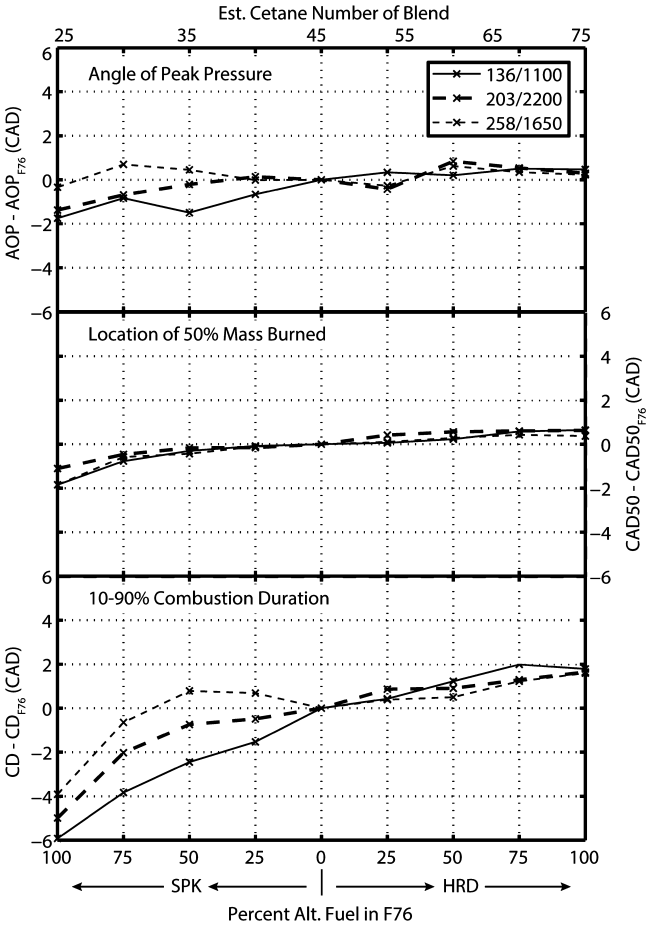

Figure 5. Combustion duration (CD, bottom), location of 50% mass fraction burned (CAD50, middle), and angle of peak pressure (AOP, top) for three different speed load points: 136 N·m/1100 rpm, 203 N·m/2200 rpm, and 258 N·m/1650 rpm. Results are reported relative to F-76 operation as a difference.

the bottom panel for three operating conditions and confirms that, in general, combustion duration increases from left-to-right along the abscissa. This trend is also reflected in the location of 50% mass fraction burned (CAD50), which is shown in the middle panel. A modest retarding of the CAD50 point is observed from left-to-right on the abscissa due to the decrease in premixed fraction and overall slower rate of combustion. However, the top panel shows that the location of peak pressure point (AOP) does not significantly or consistently change. Thus, even though the fuel is igniting sooner, the fact that it has less premixed fraction and takes longer to complete combustion results in peak pressure still occurring at essentially the same point, a trend that has been observed in other similar studies.[9]

These differences in combustion characteristics have an impact on other, more readily observable, engine operating metrics. Figure 6 shows (bottom) relative changes in peak pressure, (middle) maximum rate of pressure rise, and (top) gross indicated specific fuel consumption for the three different operating conditions. The decreased premixed fraction, slower initial combustion, longer overall combustion duration, and slightly delayed combustion phasing characteristic of the right

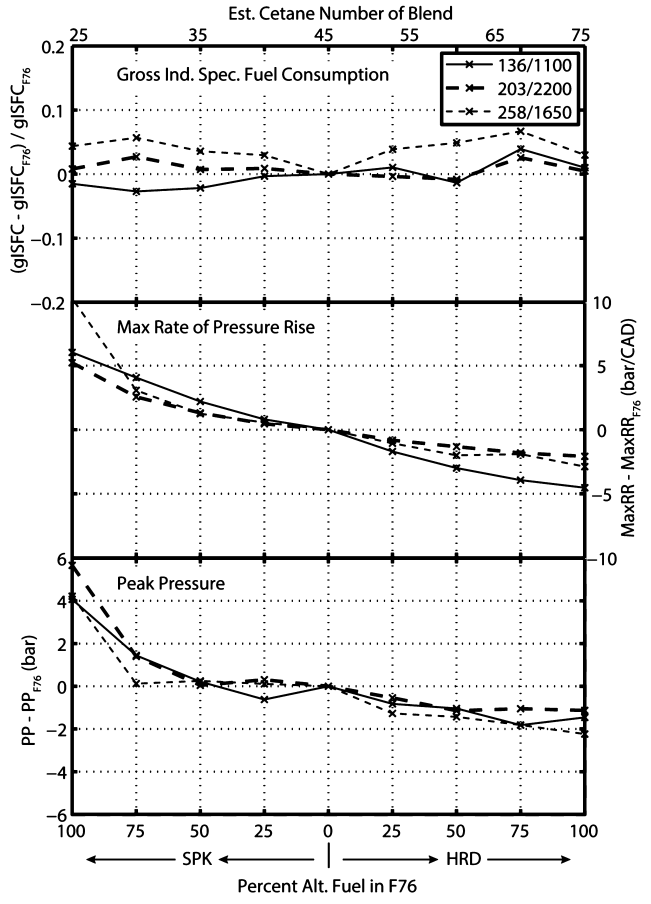

Figure 6. Peak pressure (PP, lower panel), maximum rate of pressure rise (MaxRR, middle panel), and gross indicated specific fuel consumption (gISFC, upper panel) for three different speed load points: 136 N·m/1100 rpm, 203 N·m/2200 rpm, and 258 N·m/1650 rpm. Results are reported relative to F-76 operation as a difference for PP and MaxRR and as a fraction for gISFC.

side of the Figure yields lower peak pressures (approximately 2 bar for neat HRD operation). Peak pressure is related to the peak stresses on engine components; therefore, lower peak pressures should directly translate to greater fatigue life or lower engine weight if the engine were redesigned. The lower premixed fraction and slower initial combustion rate also yield significantly lower rates of pressure rise (middle panel) by 3−5 bar/CAD. Rates of pressure are associated with vibration, noise, and also fatigue life of engine components. The upper panel of the figure shows gross indicated specific fuel consumption. For the first two operating points, there is little consistent change relative to F-76 operation; for the highest torque operating condition, an increase of 3−5% in fuel consumption over F-76 is observed, consistent with other studies.[9]

Most of these operational differences between test fuels can be connected back to IGD. Therefore, the ability to predict changes in IGD when an alternative fuel is used could prove very valuable in predicting the performance of the fuel. A detailed chemistry mechanism assembled for primary diesel reference fuels, as described in the Experimental Section, was used to model IGD. The chemistry rate equations were solved to determine the reaction rate of a parcel of fuel and air at specified *T*, *P*, and composition with constraints of constant enthalpy and pressure. The pressure was fixed at 50 bar, which is the measured pressure at SOI in the test engine. Determining

dx.doi.org/10.1021/ef500565t | *Energy Fuels* 2014, 28, 5463−5471

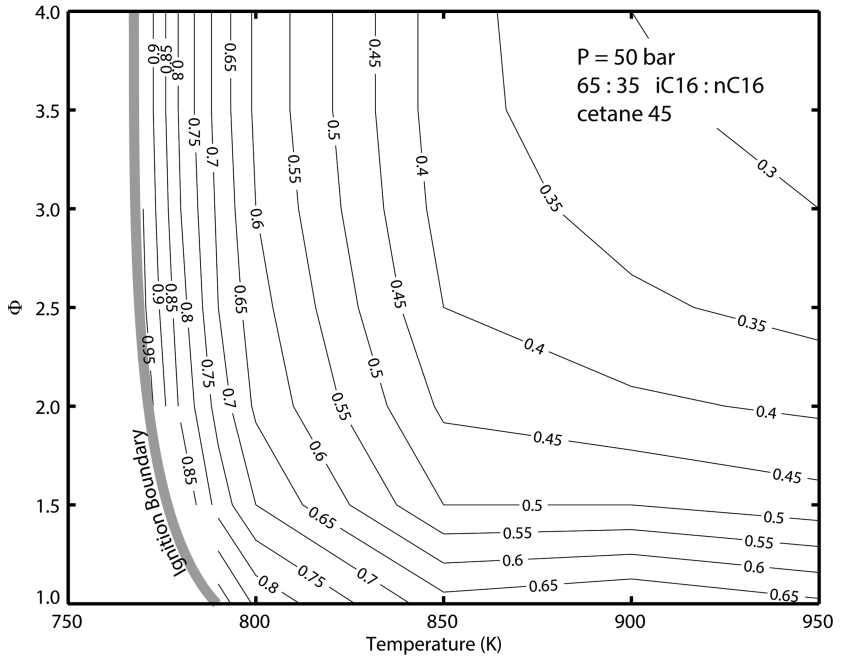

Figure 7. Modeled IGD at a range of temperatures and equivalence ratios for 65:35 blend of heptamethylnonane (i-$C_{16}H_{34}$) and normal hexadecane (n-$C_{16}H_{34}$), cetane 45, at a pressure of 50 bar.

the proper T and composition of a characteristic fuel-air parcel is difficult. One documented choice of these properties in the literature is T = 770 K, Φ = 4.0.[13,24] To explore the sensitivity of possible choices for T and Φ, the chemistry model was used to calculate IGD (based on peak CH radical concentration) for a range of T and Φ with P fixed at 50 bar and a blend of i-$C_{16}H_{34}$ (heptamethylnonane, cetane 15) and n-$C_{16}H_{34}$ (normal hexadecane, cetane 100) of 65:35 to give a cetane number of 45, characteristic of F-76.

Figure 7 shows a contour plot of this simulation with the ignition boundary shown on the left of the figure. Note that there are three regimes in this figure indicated by the slopes of the contour lines. In the upper part of the figure, at high Φ (more rich), calculated IGD is only sensitive to temperature. In the right part of the figure and at lower Φ closer to the stoichiometric point, calculated IGD is most sensitive to Φ. In the middle of the figure, at intermediate T and Φ, IGD is sensitive to both.

The temperature at SOI can be estimated from experimental data by several approaches. Figure 8 shows the calculated temperature at SOI using several different methods and assumptions. The lowest temperature, indicated as method "a" in the figure, is given by an ideal gas equation of state with a single zone model using the measured P, V, and the trapped mass estimated from the intake manifold pressure sensor. This method yields a low bound temperature because it does not account for the effect of the thermal boundary layer. For the high bound, methods "e" and "f" use an isentropic ideal gas relationship based on either a volume ratio (compression ratio, method "f") or a pressure ratio (method "e"). Both represent high bounds because they do not fully account for heat transfer during the compression stroke. Methods "b," "c," and "d" are ideal gas two-zone approaches to estimating the temperature at SOI by considering a thermal boundary layer around the combustion chamber at 400 K. The estimated temperature at SOI is then based on the mass and volume of air trapped in the core, outside the boundary layer, and the measured pressure.

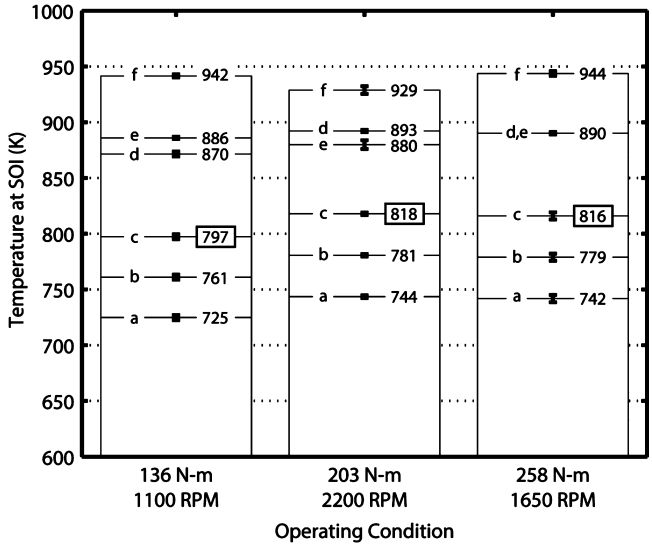

Figure 8. Experimental estimates of temperature at SOI at three different operating conditions using five methods: (a) ideal gas, single zone, using measured P and m; (d) ideal gas, two-zone (boundary layer and core), using bulk pressure and core V and m; (e) isentropic ideal gas relationship using an estimated constant specific heat and measured P ratio; (f) isentropic ideal gas relationship using an estimated constant specific heat and V ratio. Method (c) is the same as method (d) but neglects the thermal boundary layer on the piston; method (b) is 50% of method (c).

The boundary layer is approximated by the piston−cylinder clearance (given in Table 1) after Rothamer et al.[25] This piston−cylinder clearance is approximately the same as the thermal boundary layer thickness predicted from basic theory. Method "d" is the temperature predicted by this two-zone approach and, for these three operating conditions, represents approximately a 20% increase in absolute temperature from that predicted by method "a." Method "c" uses the two-zone approach but neglects the boundary layer on the piston due to

dx.doi.org/10.1021/ef500565t | Energy Fuels 2014, 28, 5463−5471

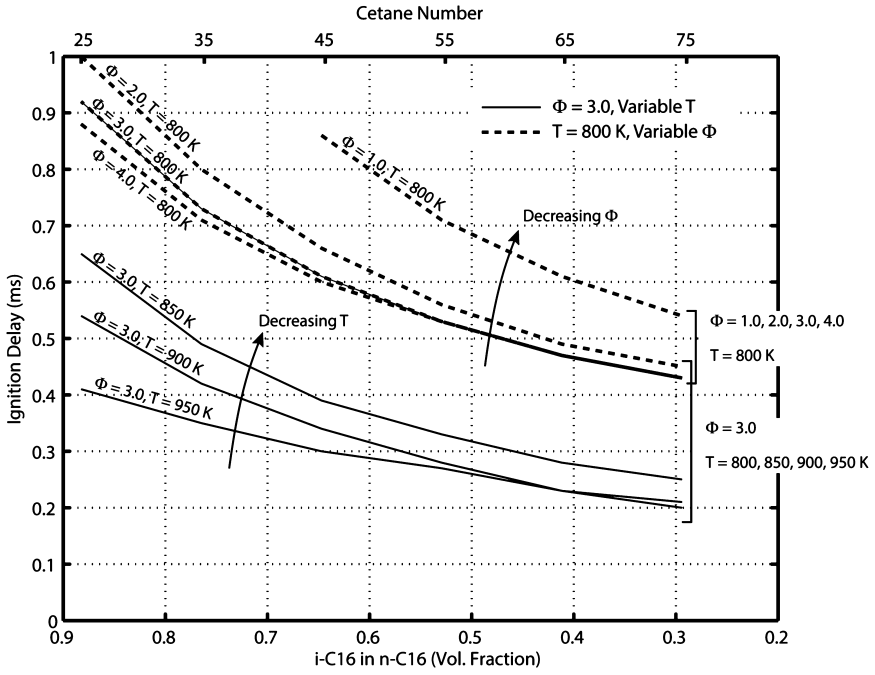

Figure 9. Modeled IGD for a range of blends of primary reference fuels heptamethylnonane (i-$C_{16}H_{34}$) and normal hexadecane (n-$C_{16}H_{34}$), parametrized by temperature (800−950 K) and equivalence ratio (2.0−4.0) at a pressure of 50 bar.

its different thermal boundary condition and results in an increase of approximately 10% relative to method "a." Method "b" is half of the change predicted by method "c" for the purposes of comparison of the methods.

As shown in Figure 8, estimated temperatures range from 725 to 744 K (lower bound) to 929−944 K (upper bound) for the three different operating points. The actual temperatures are between these bounds. Method "d" results in estimates from 870−893 K and is similar to the method used and preferred by Rothamer et al.[25] Other work by Cowart et al. on an engine with smaller bore used a two-zone approach resulting in a 10% gain, similar to the present method "c."[13] Utilizing method "c" results in T at SOI just over 800 K.

Although there is inherent uncertainty in the T at SOI values estimated here, the preceding approach provides some confidence that the actual values are between 800 and 900 K. Figure 9 shows the sensitivity of IGD predicted by the chemistry model for temperatures in this range (800, 850, 900, and 950 K) for Φ between 1 and 4 (1.0, 2.0, 3.0, 4.0) as a parametric plot. At each point in this plot, the composition of primary reference fuel in the model is adjusted to approximately match the cetane number of the experimentally tested fuel blend, and this composition is shown on the horizontal axis. The solid lines represent the effect of T changes at fixed Φ = 3.0. The dashed lines represent the effect of Φ changes at fixed T of 800 K. The primary reference fuel composition is adjusted to achieve cetane numbers from 25 to 75, representative of the range of fuel blends experimentally tested in this study. The figure immediately shows that IGD is sensitive to both T and Φ changes, although the differences get smaller for high cetane numbers. Thus, to create a representative model, the choice of T and Φ is not trivial.

Despite the apparent sensitivity shown in Figure 9, the trends of IGD do appear to have a similar shape, suggesting that it may be possible to use the model to predict relative trends despite uncertainty in the proper choice of T and Φ. Figure 10 shows

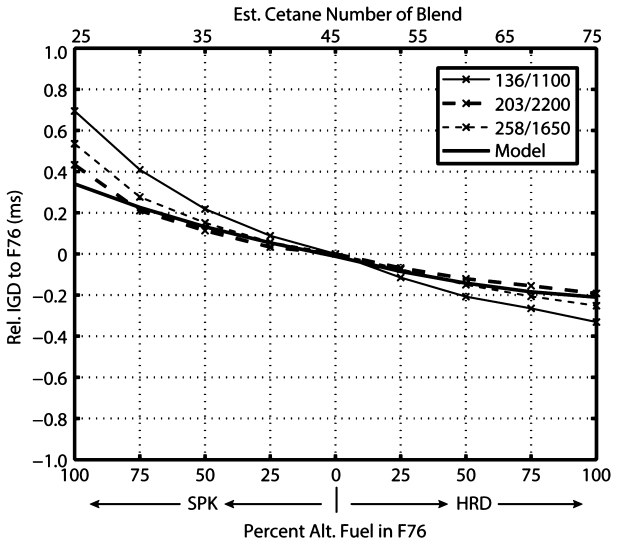

Figure 10. Comparison of experimental data at three operating conditions (trends with "×" data markers) with the PRF model (solid, bold trend line) for IGD relative to F-76 operation. Model values are for P = 50 bar, T = 800 K, Φ = 2, with ratio of i-$C_{16}H_{34}$ to n-$C_{16}H_{34}$ chosen to nominally match cetane number for each mixture of SPK and HRD with F-76.

an example of this approach. Here, the chemistry model is used to predict IGD at T = 800 K and Φ = 2.0, choices that are consistent with the T at SOI estimation described in connection with Figure 8. The modeling results are converted to a relative basis by referencing the predicted IGD at each point to that for a primary reference fuel blend at 45 cetane number. This relative modeling result is shown in Figure 10 as a solid bold line. The modeling result shows excellent agreement with experimental trends, particularly for the highest power (203 N·m/2200 rpm) and highest torque (258 N·m/1650 rpm) operating points.

dx.doi.org/10.1021/ef500565t | Energy Fuels 2014, 28, 5463−5471

SUMMARY AND CONCLUSIONS

Blends of SPK and HRD fuels with F-76 were tested in a direct injection marine diesel engine. Satisfactory operation was achieved for all tested fuel blends, but important performance differences were observed. Since SPK has a very low cetane number (25), increasing amounts of SPK with F-76 results in increases in IGD. In contrast, since HRD has a high cetane number around 75, increasing amounts of HRD with F-76 results in decreasing IGD. As IGD gets shorter, premixing of air and fuel decreases, and the rapid premixed combustion phase is reduced, resulting in overall lengthening of the combustion duration and retarding of the 50% mass fraction burned point. These two effects (shorter IGD and longer combustion duration) are mutually offsetting for the location of peak pressure, such that the angle of peak pressure remains largely unchanged for any tested fuel blend.

The effects of decreased IGD result in lower peak pressure and rates of pressure rise. These operational parameters can be related to structural fatigue life, noise, and vibration of the engine. Therefore, operation with high levels of HRD could result in improvements in these operational metrics. Measurement of gross indicated specific fuel consumption shows mixed results; depending on operating conditions, a 0−5% increase in fuel consumption was observed.

The two alternative fuels tested in this study are both highly paraffinic fuels but show different autoignition qualities, and blends with F-76 result in a wide range of cetane numbers from 25−75. A diesel primary reference fuel model of chemistry reaction rates was used to determine if and how it could be used to predict ignition trends of the alternative fuels tested experimentally in this study. The model was used to calculate IGD of an air-fuel parcel at P = 50 bar, variable T and Φ, and composition of i-$C_{16}H_{34}$ and n-$C_{16}H_{34}$ to approximately match the cetane number of the experimental fuel blend of SPK/HRD with F-76. The best estimates of T at SOI result in values between 800−900 K, and in this range, the model shows sensitivity to both T and Φ. However, calculated IGD trends are largely self-similar, and when converted to a relative basis, the model shows excellent agreement with experimental trends. Thus, the diesel primary reference fuel chemistry model was able to predict changes in IGD using a characteristic air-fuel parcel temperature of 800 K and Φ = 2.0. Since the chemistry model alone was able to capture the essential trends of IGD changes with fuel type, it is unlikely that other fuel property differences, for example, ones that affect diesel spray development (viscosity, surface tension, density), have a significant and net effect on overall IGD.

The exact composition of future alternative fuels is uncertain, so the possibility of using a standard primary reference fuel model to predict basic operational parameters such as IGD is promising. The IGD can, in turn, be used to provide qualitative or even quantitative prediction of other operational parameters such as peak pressure, maximum rate of pressure rise, or the general viability of the fuel in a diesel engine. Thus, this study demonstrates one way that that IGD changes could be predicted simply using currently available primary reference fuel chemistry models.

AUTHOR INFORMATION

Corresponding Author

*E-mail: patcaton@usna.edu. Phone: (410) 293-6516.

Present Address

[†]Department of Mechanical Engineering, U.S. Naval Academy, 590 Holloway Road, Annapolis, MD 21402.

Notes

The authors declare no competing financial interest.

ACKNOWLEDGMENTS

This study was supported by the Office of Naval Research as part of the Alternate Naval Fuels Program under the cognizance of Dr. S. Beerman-Curtin via funding document N0001413WX20922. The authors also acknowledge the excellent support of Mr. A. Paz in laboratory data collection.

ABBREVIATIONS

AOP = crank angle of peak pressure
ATC = after top-center
BTC = before top-center
CAD = crank angle degree
CAD10 = crank angle degree location of 10% mass fraction burned
CAD50 = crank angle degree location of 50% mass fraction burned
CAD90 = crank angle degree location of 90% mass fraction burned
CD = combustion duration
c_v = specific heat at constant volume
F-76 = petroleum-based military diesel fuel
FAMES = fatty-acid methyl esters
FT = Fischer−Tropsch
gISFC = gross indicated specific fuel consumption
HMMWV = high mobility multipurpose wheeled vehicle
HRD = hydrotreated renewable diesel
IGD = ignition delay
LHV = lower heating value
m = mass
MaxRR = maximum rate of pressure rise
P = pressure
PP = peak pressure
RPM = revolutions per minute
SOI = start of injection
SOC = start of combustion
SPK = synthetic paraffinic kerosene
T = temperature
V = volume
Φ = fuel-air equivalence ratio

REFERENCES

(1) Fiscal Year 2011 Operational Energy Annual Report, Technical Report 3-F901A9C for the U.S. Department of Defense: Arlington, VA, March 2013.

(2) Energy. U.S. Department of the Navy Energy, Environment, and Climate Change. http://greenfleet.dodlive.mil/energy/ (accessed May 10, 2013).

(3) Bartis, J. T. and Bibber, L. V. *Alternative Fuels for Military Applications*. http://www.rand.org/pubs/monographs/MG969.html (accessed May 13, 2011).

(4) Anderson, L. L.; Tillman, D. A. Light Liquids and Chemicals from Coal. In *Synthetic Fuels from Coal;* John Wiley & Sons: Hoboken, NJ, 1979; pp 122−135.

(5) Mikkonen, S. Second-Generation Renewable Diesel Offers Advantages. *Hydrocarbon Process.* **2008**, *87*, 63−66.

(6) Sugiyama, K.; Goto, I.; Kitano, K.; Mogi, K.; Honkanen, M. Effects of Hydrotreated Vegetable Oil (HVO) as Renewable Diesel

Fuel on Combustion and Emissions in Diesel Engine. *SAE Int. J. Fuels Lubr.* **2012**, *5*, 205−217.
(7) Kuronen, M.; Mikkonen, S.; Aakko, P.; Murtonen, T. Hydrotreated Vegetable Oil as Fuel for Heavy-Duty Diesel Engines. *SAE Technical Paper 2007−01−4031;* SAE International: Troy, MI, 2007.
(8) Aatola, H.; Larmi, M.; Sarjovaara, T.; Mikkonen, S. Hydrotreated Vegetable Oil (HVO) as a Renewable Diesel Fuel: Trade-off between NOx, Particulate Emission, and Fuel Consumption of a Heavy Duty Engine. *SAE Int. J. Engines* **2009**, *1*, 1251−1262.
(9) Caton, P. A.; Williams, S. A.; Kamin, R. A.; Luning-Prak, D.; Hamilton, L. J.; Cowart, J. S. *Hydrotreated Algae Renewable Fuel Performance in a Military Diesel Engine.* ICED Spring Technical Conference, Torino, Italy2012, ASME: New York, NY, 2012; p 81048.
(10) Cowart, J.; Carr, M.; Caton, P.; Stoulig, L.; Luning-Prak, D.; Moore, A.; Hamilton, L. High Cetane Fuel Combustion Performance in a Conventional Military Diesel Engine. *SAE Int. J. Fuels Lubr.* **2011**, *4*, 34−47.
(11) Olree, R. M.; Lenane, D. L. *Diesel Combustion Cetane Number Effects;* International Congress and Exposition, Detroit, MI, 1984, ASME: New York, NY, Feb 27−Mar 2, 1984.
(12) Caton, P. A.; Hamilton, L. J.; Cowart, J. S. Understanding Igntion Delay Effects With Pure component Fuels in a Single-Cylinder Diesel Engine. *J. Eng. Gas Turbines Power* **2011**, *133*, 032803−032811.
(13) Cowart, J.; Raynes, M.; Hamilton, L.; Luning-Prak, D.; Mehl, M.; Pitz, W. J. *An Experimental and Modeling Study into Using Normal and Iso Cetane Fuel Blends as a Surrogate for a Hydro-Processed Renewable Diesel (HRD) Fuel.* ICED Fall Technical Conference, Detroit, MI, Offer ICEF2013−19056, 2013; ASME: New York, NY, 2013.
(14) Westbrook, C. K.; Pitz, W. J.; Mehl, M.; Curran, H. J. Detailed Chemical Kinetic Reaction Mechanisms for Primary Reference Fuels for Diesel Cetane Number and Sprak-Ignition Octane Number. *Proc. Combust. Inst.* **2011**, *33*, 185−192.
(15) Westbrook, C. K.; Pitz, W. J.; Herbinet, O.; Curran, H. J.; Silke, E. J. A Detailed Chemical Kinetic Reaction Mechanism for n-Alkane Hydrocarbons from n-Octane to n-Hexadecane. *Combust. Flame* **2009**, *156*, 181−199.
(16) Sarathy, S. M.; Westbrook, C. K.; Mehl, M.; Pitz, W. J.; Togbe, C.; Dagaut, P.; Wang, H.; Oehlschlaeger, M. A.; Niemann, U.; Seshadri, K.; Veloo, P. S.; Ji, C.; Egolfopoulos, F. N.; Lu, T. Comprehensive Chemical Kinetic Modeling of the Oxidation of 2-Methylalkanes From C7 to C20. *Combust. Flame* **2011**, *158*, 2338−2357.
(17) Sarathy, S. M.; Yeung, C.; Westbrook, C. K.; Pitz, W. J.; Mehl, M.; Thomson, M. J. An Experimental and Kinetic Modeling Study of *n*-Octane and 2-Methylheptane in an Opposed-Flow Diffusion Flame. *Combust. Flame* **2011**, *158*, 1277−1287.
(18) Goodwin, D. G. An Open-Source, Extensible Software Suite for CVD Process Simulation. In *Chemical Vapor Deposition XVI and EUROCVD 14, ECS Proceedings 2003, 2003−08,* Allendorf, M., Maury, F., Teyssandier, F., Eds.; The Electrochemical Society: Pennington, NJ, 2003; pp 155−162.
(19) Sihling, K.; Woschni, G. Experimental Investigation of the Instantaneous Heat Transfer in the Cylinder of a High-Speed Diesel Engine. In *SAE Technical Paper 790833;* SAE International: Warrendale, PA, 1979.
(20) Smith, G. P.; Golden, D. M.; Frenklach, M.; Moriarty, N. W.; Eiteneer, B.; Goldenberg, M.; Bowman, C. T.; Hanson, R. K.; Song, S.; Gardiner, W. C. Jr.; Lissianski, V. V.; Qin, Z. http://www.me.berkeley.edu/gri_mech/ (accessed August 2013).
(21) Gatowski, J. A.; Balles, E. N.; Chun, K. M.; Nelson, F. E.; Ekchian, J. A.; Heywood, J. B. Heat Release Analysis of Engine Pressure Data. *SAE Int. J. Engines* **1984**, 5961−5977.
(22) Chun, K. M.; Heywood, J. B. Estimating Heat-Release and Mass-of-Mixture Burned from Spark-Ignition Engine Pressure Data. *Combust. Sci. Technol.* **1987**, *54*, 133−143.
(23) Mathes, A.; Ries, J.; Caton, P.; Cowart, J.; Luning Prak, D.; Hamilton, L. Binary Mixtures of Branched and Aromatic Pure Component Fuels as Surrogates for Future Diesel Fuels. *SAE Int. J. Fuels Lubr.* **2010**, *3*, 794−809.
(24) Curran, H. J.; Fisher, E. M.; Glaude, P.-A.; Marinov, N. M.; Pitz, W. J.; Westbrook, C. K.; Layton, D. W.; Flynn, P. F.; Durrett, R. P.; Loyze, O. Z.; Akinyemi, O. C.; Dryer, F. L. Detailed Chemical Kinetic Modeling of Diesel Combustion with Oxygenated Fuels. In *SAE Technical Paper 2001−01−0653;* SAE International: Troy, MI, 2001.
(25) Rothamer, D. A.; Murphy, L. Systematic Study of Ignition Delay for Jet Fuels and Diesel Fuel in a Heavy-Duty Diesel Engine. *Proc. Combust. Inst.* **2013**, *34*, 3021−3029.